

Low temperature growth of nanocrystalline diamond: Insight thermal property

J. Millán-Barba^{a,*}, A. Taylor^b, H. Bakkali^a, R. Alcantara^c, F. Lloret^d, R. Guzmán de Villoria^e, M. Domínguez^f, V. Mortet^b, M. Gutiérrez^a, D. Araújo^a

^a Dep. Materials Science and Metallurgical Engineering and Inorganic Chemistry, University of Cadiz, Spain

^b Dep. of Functional Materials, Institute of Physics of the Czech Academy of Sciences, Czech Republic

^c Dep. of Physical Chemical, University of Cádiz, Spain

^d Department of Applied Physics, University of Cádiz, Spain

^e FIDAMC, Foundation for Research, Development and Application of Composite Materials, Spain

^f Dep. Condensed Matter Physics and Institute of Research on Electron Microscopy and Materials, University of Cadiz, Spain

ABSTRACT

One of the limitations of materials for high-power devices and structural coatings applications is heat dissipation. Diamond is a suitable material for heat distribution due to its high thermal conductivity. Nevertheless, it is usually grown at high temperature (800–1200 °C), which limits its use as a coating for substrates vulnerable to degradation at high temperatures. In this work, it is studied the effect of the distance between the plasma source and substrate on the growth of nanocrystalline diamond layers on silicon substrates at low temperature (<450 °C) by microwave linear antenna plasma enhanced chemical vapour deposition (MW-LA-PECVD) in pulse mode. The nanocrystalline diamond films have been analysed by scanning electron microscopy (SEM), atomic force microscopy (AFM) and Raman spectroscopy. Finally, the superficial thermal conductivity of the diamond layers was determined by scanning thermal microscopy-AFM (SthM-AFM).

1. Introduction

Diamond is widely used as a coating and substrate for several applications such as electronic, electrochemistry, biomedical, cutting and abrasive or composite material [1–6]. This is due to diamond's excellent mechanical, optical, and thermal properties, as well as its biocompatibility and non-toxicity [7]. Intrinsic diamond is an electrical insulator, but it can be modified by dopants to obtain semiconductor properties, i.e. boron or phosphorus [8].

Microwave plasma enhanced chemical vapour deposition (MPCVD) and hot filament chemical vapour deposition (HFCVD) systems are the most common way to grow synthetic diamond films. However, these systems cover relatively small coating areas at high temperatures (600–1000 °C) [9,10], which limits the substrate material and hence potential applications [11]. Even when diamond epitaxial layers are grown, the different coefficient of thermal expansion between the diamond layer and the substrate triggers the break-up of the layer during cooling. Making more efficient growths by keeping the substrate temperature low is an advantage in manufacturing. So that internal stresses between the substrate and the diamond due to thermal shrinkage during

cooling do not cause the layer to break.

Notwithstanding the difficulties, M. Ihara et al. achieved diamond growth at 135 °C by HFCVD with a sample water cooling system, although only dispersed micro-diamond grains could be obtained [12]. Other authors achieved inhomogeneous layers of non-well faceted diamond below 300 °C by adding H₂S to the gaseous precursor mixture in a HFCVD [13]. Nevertheless, diamond growth at low temperature by HFCVD entails drawbacks such as contamination of impurities from the filaments, small deposition areas or low growth rates.

In this context, begins to increase research and use of CVD systems that would allow growth at low temperatures and over large areas. For instance, microwave linear antenna plasma enhanced chemical vapour deposition system (MW-LA-PECVD) allows low temperatures (300–600 °C) and large-area (>50 cm × 30 cm) of nanocrystalline diamond (NCD) growth [14]. Low temperature diamond growth processes allow to grow on low-melting point substrates. This opens up a wide range of applications and, together with the modular design of MW-LA-PECVD system, makes it scalable to large areas and suitable for industrial production.

Diamond growth is widely reported by MW-LA-PECVD systems, as

* Corresponding author at: Universidad de Cádiz, Dpto. Ciencias de los Materiales e Ingeniería Metalúrgica y Química Inorgánica, CASEM, Despacho 23, Pala A, 1ª planta, Avda. República Saharaui, s/n, CP:11510 Puerto Real, Cádiz, Spain.

E-mail address: josue.millan@gm.uca.es (J. Millán-Barba).

<https://doi.org/10.1016/j.diamond.2023.110070>

Received 1 December 2022; Received in revised form 23 May 2023; Accepted 27 May 2023

Available online 1 June 2023

0925-9635/© 2023 The Authors. Published by Elsevier B.V. This is an open access article under the CC BY license (<http://creativecommons.org/licenses/by/4.0/>).

well as the influence of gases ratio ($\text{CO}_2/\text{CH}_4/\text{H}_2$) and how CO_2 significantly improve the quality and diamond growth rate. By this technique, the diamond grain size can be controlled by varying the pressure [15]. Authors also reported NCD growth at 450°C in a $30 \times 30 \text{ cm}^2$ area using coaxial plasma line sources to ensure a uniform and stable plasma over such large areas by MW-LA-PECVD [16]. Even NCD growth by MW-LA-PECVD at lower temperatures (400°C) has been reported, using a precursor gas ratio composed of $\text{CO}_2/\text{CH}_4/\text{H}_2$. S. Drijkoningen et al. proposed potential mechanisms of NCD growth [17] and J. Zalieckas et al. showed the feasibility of NCD as a coating for orthopaedic implants due to the ability of this material to generate osteogenic cell proliferation [18].

In addition, alternative methods with the aim of decreasing the NCD growth temperature are proposed by other authors. J. Kim et al. used microwave antennas with annular multi-slots to irradiate microwaves in all directions in MW-LA-PECVD systems. This improvement enables the deposition of large areas ($300\text{--}600 \text{ mm}^2$) at temperature as low as 300°C [19]. Other alternative system produces microwaves from solid-stated generators in distributed antenna array. In which NCD growth was reported at 250°C , at the cost of a low growth rate ($15\text{--}17 \text{ nm/h}$) [20]. Recently, NCD have been obtained at 395°C of growth temperature with 80 nm/h growth rate by using composite right/left-handed material as a slotted waveguide [21]. Despite existing knowledge, low temperature growths are most affected by the growth conditions, especially when doping elements are introduced in the precursor gases to achieve higher electrical properties in diamond.

Growth of boron-doped diamond (BDD) at low temperature is a difficult task, which requires low pressure (1 mbar), low electron temperature ($<5 \text{ eV}$) and high plasma density ($>10^{11}/\text{cm}^{-3}$) [22,23]. Boron-doped diamond can be deposited using MW-LA-PECVD, however, the gas composition not only controls the concentration of impurities, but also modifies the diamond growth rate and grain size [24].

BDD is a suitable material for different semiconductor applications, as for example electrical capacitor, and electrodes resistant to aggressive or biological environments, due to its wide bandgap and high electrical conductivity [7,25–27]. Therefore, low-temperature BDD growth can be used to improve mechanical and electrical properties as a coating on a wide range of low melting point materials, as well as providing biocompatibility and corrosion resistance properties.

In addition to the semiconducting properties of the BDD coatings, the heat dissipation of diamond supposes a necessary quality during working processes to maintain the reliability and performance of the devices [28–30]. Polycrystalline diamond has a very high thermal conductivity ($1300\text{--}2000 \text{ W/m}\cdot\text{K}$) [31], but thermal properties decrease with the doping concentration and the grain size in doped polycrystalline diamond films. Previous studies on polycrystalline diamond established a dependence between grain size and thermal conductivity [28]. The microstructure of polycrystalline diamond is responsible for phonon scattering and defect accumulation at grain boundaries. Therefore, thermal conductivity of polycrystalline diamond is reduced with respect to single crystal diamond. BDD with nanocrystalline grain size ($10^1\text{--}10^2 \text{ nm}$) has been characterized by Raman thermography or Laser Flash Technique, obtaining a thermal conductivity ranging from a few $\text{W/m}\cdot\text{K}$ to a few hundred $\text{W/m}\cdot\text{K}$ [28,32].

This work relates nanostructure and thermal conductivity of NCD films grown on Si wafers. NCD was grown on several samples by MW-LA-PECVD at different substrate-to-antenna distance (SAD). During diamond growth and with the aim of doping it, a boron precursor (diborane) has been used in the gas mixture. The NCD structural and thermal consequences of such SAD variation are also discussed in this study. Quality of the deposited diamond/non-diamond (sp^3/sp^2 ratio carbon bonds) has been evaluated. SAD dependence has been investigated by scanning electron microscopy (SEM), atomic force microscopy (AFM), Raman spectroscopy and scanning thermal microscopy-AFM (SThM-AFM).

2. Methodology

NCD films have been grown on Si substrates in a MW-LA-PECVD system. Si substrates were diamond seeded prior to deposition with nanodiamond particles with an average size of $4\text{--}6 \text{ nm}$ deposited by electrospray [33]. Diamond growth was carried out using a 200 sccm of total gas flow was used in a mixture which consisted of: $3\% \text{ CH}_4$, $25\% \text{ B}_2\text{H}_6$ (0.75% in hydrogen) and $1\% \text{ CO}_2$, diluted in H_2 . Working pressure and microwave power were set at 0.25 mbar and 7.5 kW in pulse mode, respectively. Microwave sources were set in pulse mode at 303 Hz pulse frequency, with a time ON and OFF of 1 ms and 2.3 ms , respectively, and a duty cycle of 30% . Growth process time was 8 h . Ten Si substrates were placed at different SAD in 0.5 cm intervals from 7.5 to 12 cm . Samples are named by their SAD value. This means on samples #7.5, #8..., #11.5, #12 where only the SAD (cm) vary. The sample growth temperature was below the minimum measurable temperature of the pyrometer (Williamson Pro 92 38), i.e., lower than 450°C . The stage was not heated. Therefore, the temperature of the samples decreases with their SAD. In this way, the sample closest to the plasma source (SAD #7.5) showed the highest surface temperature (lower than 450°C) measured by a laser pyrometer.

The thicknesses of the deposited layers were measured by focused ion beam scanning electron microscopy (FIB-SEM) using a Solaris Tescan UHR FESEM FIB microscope. First, FIB was used to deposit a thin layer of platinum. Then, a square area of $15 \mu\text{m} \times 6 \mu\text{m}$, and $3 \mu\text{m}$ depth was etched away delimited by the deposited Pt. The sample was tilted and observed by SEM enabling measurement of the thickness of the deposited diamond layer. The same microscope was used for the study of the morphology and the surface roughness at 15 kV of accelerating voltage.

To determine the sp^3/sp^2 carbon bond content, Raman spectra were collected in a backscattered geometry using a Horiba LabRAM Evolution spectrometer with a 473 nm laser excitation source and a $\times 100$ objective lens with $1800 \text{ lines mm}^{-1}$ grating. To differentiate the peaks and bands of the Raman spectra. They were deconvoluted including the signal of the boron band, diamond peak, D-band, G-band, ν_1 and ν_3 trans-polyacetylene peaks typically found in CVD diamond growth with boron inclusions [34]. Multiplex deconvolution were carried out using Lorentzian function.

Topography and thermal conductivity in the samples were recorded simultaneously in areas of $20 \times 20 \mu\text{m}^2$ by contact SThM-AFM. A VITA-DM-GLA-1 tip from Bruker was used with a temperature resolution of 0.1°C and lateral resolution better than 100 nm . Measurements were carried out in contact mode with a scan rate was 0.4 Hz and a 1 V applied in the tip, to scan the sample surface and map qualitative variations in the thermal conductivity of the sample. The scan angle was 90° to better preserve the integrity of the tip after multiple scans. This combination of techniques gives the user visual and property-based information on a sub-micrometre scale.

3. Results

Morphology and roughness of the samples grown by MW-LA-PECVD were observed by SEM and AFM. The thickness of the deposited layers has been estimated in cross-section view by FIB-SEM. Fig. 1 shows SEM micrographs of samples #7.5, #8, #9, #10, #11 and #12 cm. All samples showed nanocrystalline cauliflower shaped structures with cavities between the grains, in no case do the cavities reach the substrate. Previous studies showed that at temperatures higher than 650°C and B/C rates of about $15,000 \text{ ppm}$, micro-sized diamond grains can be obtained [35]. In this work, growth is carried out at lower temperatures ($<450^\circ\text{C}$) leading to reduced growth rates [36]. As result unfaceted grains are obtained for all samples.

The growth process resulted in very different layer thicknesses and uniformities. It is compared fully closed films with almost bare substrate in some cases which is not fully correct. In other cases films of different

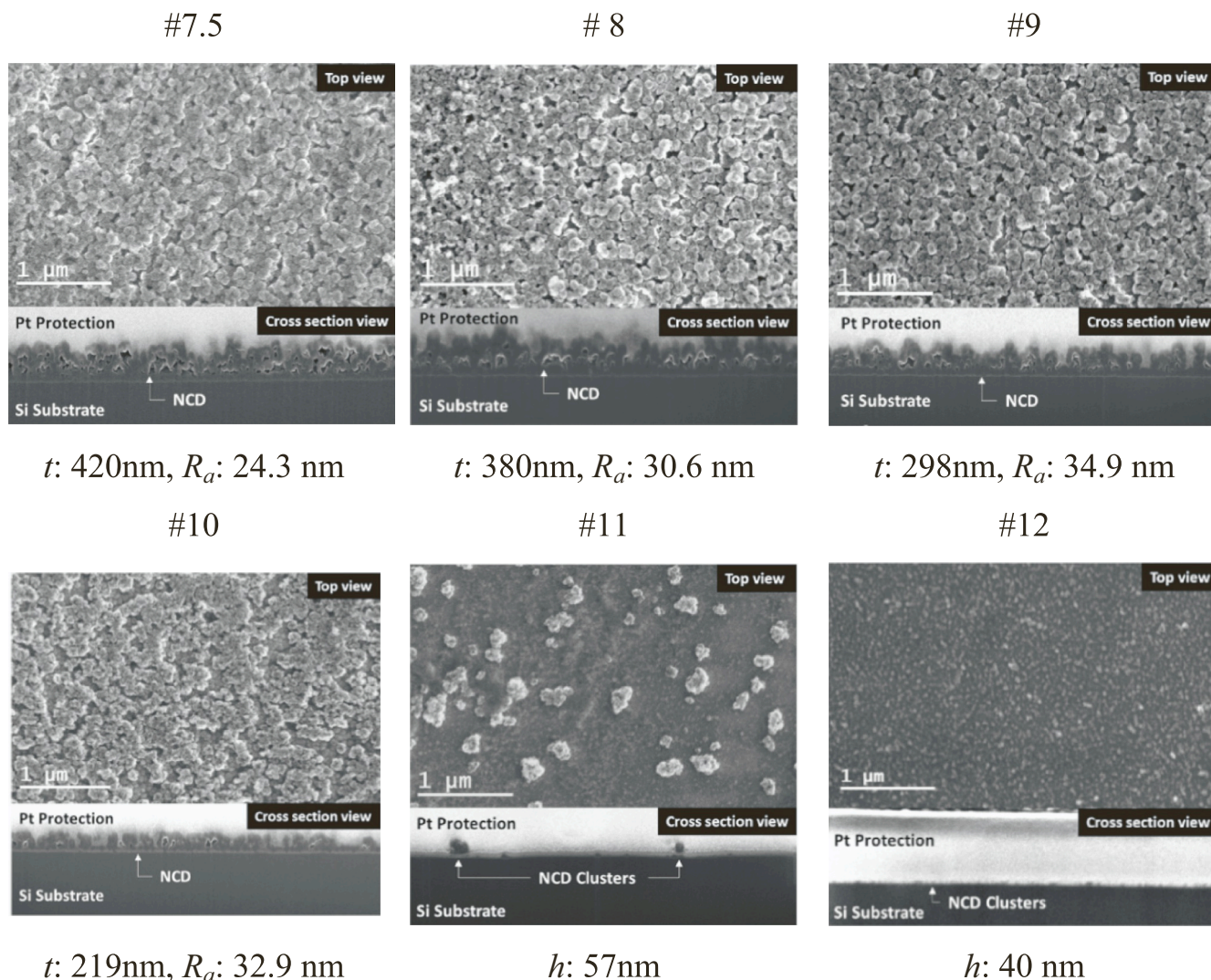


Fig. 1. SEM micrographs of nanocrystalline diamond layers, top view (up) and cross-section (down), as a function of the substrate-to-antenna distance (SAD). Thickness (*t*) of the layers is indicated in each sample. Roughness (*R_a*) of the layers and grain height (*h*) of the isolated clusters (#11 and #12) are included in the figure were obtained by AFM.

thickness are compared despite that properties can be dependent on it as for example roughness, *R_a*. Therefore, deductions should be carried out with the utmost prudence. Having this in mind, the following observations can be made.

There is a linear trend of thickness (*t*) decreasing from sample #7.5 to #10, starting at 420 nm and ending at 219 nm, respectively. However, from sample #11 there is an abrupt decrease of the growth tentatively due to the reduction of the plasma density. At relatively long distances the number of excited species (atomic hydrogen and CH_x species) is low [37,38]. Thus, only isolated clusters (~50–40 nm) of cauliflower nanocrystalline grains are observed in sample beyond #11, together large smooth areas with no diamond deposition.

Roughness measurements are not related to grain morphology, but to growth inhomogeneity (Fig. 1). The cauliflower NCD clusters deposition generates a rough surface. Thicker samples resulted in a higher homogeneity of the surface and therefore in a lower *R_a*. For samples beyond #11, only the mean cluster heights are given (*h*).

Fig. 2 shows a decrease in NCD growth rate with SAD. Higher diamond growth rate is obtained at SAD of 7.5 cm, ~50 nm/h. From there on a linear decreasing trend is observed until sample #10.5. In samples at #11 onwards, the growth rate decreases sharply to ~5 nm/h, tending asymptotically to zero. So, from this distance (#11) the plasma density decreases drastically indicating its limit (not shown in Fig. 2). This is in

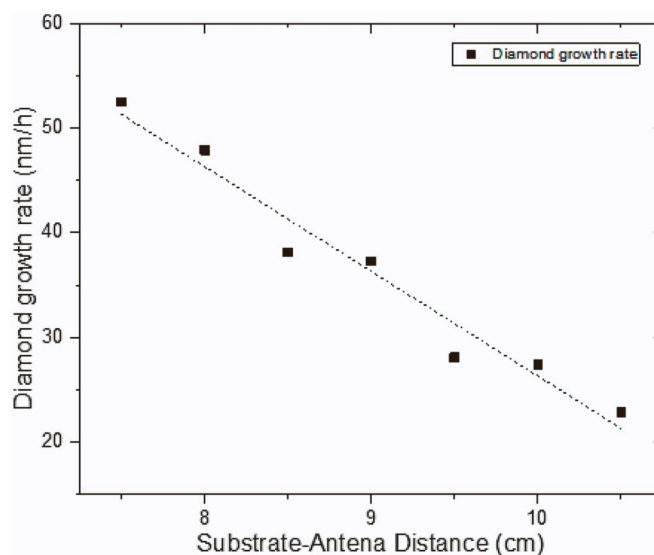


Fig. 2. Diamond growth rate as function of the growth SAD.

concordance with previous reports on MW-LA-PECVD diamond growth [24,35].

The diamond phase on the grown layer have been evaluated by Raman spectroscopy. Fig. 3 shows the Raman spectra of the samples ordered according to their SAD. All sample were included in Fig. 3 to evaluate the diamond quality. For the acquisition of Raman spectra on samples #11 onwards, the laser was focused on diamond clusters. Samples with lower SAD show the diamond peak (sp^3 carbon bonds) at 1325 cm^{-1} displaced from its usual position, 1332 cm^{-1} . This displacement to lower energies is a consequence to a content of boron in the NCD layers, which produces a broad band around the 1200 cm^{-1} position [39,40]. This boron related broad band at 1200 cm^{-1} is not clearly distinguishable at lower SAD (#7.5, #8, #8.5 and #9), as a slight shoulder to the left of the diamond peak is observed (1240 cm^{-1}). Samples grown at large distances (samples #10.5 to #12) also show a displaced wide diamond peak, although boron incorporation is not evidenced. This is due to the low Raman signal and a higher amount of amorphous carbon resulting in poor detection and a weaker diamond peak. A broad peak associated with transpolyacetylene (v_3 T-Trans) from the grain boundaries is shown at 1490 cm^{-1} in all the samples [41]. This peak is sharper in samples #11 to #12, indicating a higher percentage of sp^2 carbon. The G band, which is related with graphitic sp^2 bond is usually observed at 1580 cm^{-1} . However, in samples #11 to #12, the G-band is shown at 1550 cm^{-1} . This displacement is due to the amorphization since the sp^2 bonds are weakened and softening of the vibrations modes [42–44]. The D-band typically observed at 1350 cm^{-1} is not clearly distinguishable in all samples. This band is related to graphitic sp^2 bonds. Even if the peak is not clearly observed, it is used in subsequent calculations to deconvolute the peaks [45]. As the SAD increases, the D-band and the v_1 transpolyacetylene band are observed

around 1350 cm^{-1} and $1100\text{--}1200\text{ cm}^{-1}$, respectively (from sample #10.5 to #12). This is attributed to a higher content of sp^2 carbon bonds at these SAD.

For sp^3/sp^2 ratio calculation, peak intensities areas of diamond, G-band, and D-band from Raman spectrum results were used (an example of Raman multipeak deconvolution using Lorentzian function is shown in the Raman spectrum of sample #7.5 in Fig. 3). The sp^3/sp^2 ratio obtained in all samples remains above 90 %, which is in agreement with results obtained in other research depositions [35,46].

Fig. 4a shows topographical overlayed with the colour thermal conductivity map of NCD layers (in purple) on a silicon substrate (in yellow) by SThM-AFM. Silicon substrate is used as a thermal reference. The scan was performed in a region prepared by Focus Ion Beam (FIB) enabling comparison of the thermal response of the NCD with that of silicon. The deposited diamond surface exhibits granular roughness, characteristic of the cauliflower NCD observed in Fig. 1. Silicon substrate has a smooth surface resulting from the ion-milling. Thermal conductivity maps are obtained from the SThM tip resistance variation, which is proportional to the output voltage of a Wheatstone bridge, where the tip resistance is the unknown value. Since the Wheatstone bridge is balanced before the tip contacts the sample surface and the scanning begins, its output voltage variations during sample scanning, presented in Fig. 4 as a colour scale map, are proportional to the tip resistance. Because the SThM tip is made of a thin metallic film, the higher its resistance the higher its temperature. A higher tip temperature (i.e., a higher output voltage) means a lower thermal conductivity of the sample surface it is scanning, given the fact that the tip is always at a higher temperature than the sample. This is due to Joule self-heating and the heat flows from the tip to the sample. So, violet-blue areas correspond to lower thermal conductivity (NCD layer) while higher thermal conductivity areas appear in green-yellow colour (Si substrate).

The thermal response of the NCD layers as function of the SAD are shown in Fig. 4b. Samples at #11 onward are not included in thermal study due to the absence of a continuous layer. Both regions show homogenous thermal conductivity in all the samples (Fig. 4b). Thermal conductivity maps distributions have been fitted to a double Lorentzian function. Average values of the fitted curves were used to estimate the thermal conductivity of NCD layers by the Eq. (1) using the silicon value, $\lambda_{Si} = 200\text{ W/m}\cdot\text{K}$, as a reference. These are shown in Table 1.

$$\lambda_{NCD} = \frac{\lambda_{Si} \times M_{Si}}{M_{NCD}} \quad (1)$$

where λ_{NCD} is the NCD thermal conductivity, λ_{Si} is the silicon thermal conductivity, and M_{Si} and M_{NCD} are the distribution mode from SThM-AFM maps of the silicon and NCD area, respectively. Thermal conductivity estimation of nanocrystalline NCD remains constant for all samples in the range of $\lambda_{NCD} = 10^2\text{ W/m}\cdot\text{K}$. Therefore, it is independent of the SAD and the diamond thickness. Therefore, the thermal conductivities of NCD grown at low temperature by MW-LA-PECVD show a similar thermal conductivity to that of NCD grown by MWPECVD and HFCVD, previously reported by the literature ($50 > \lambda < 500\text{ W/m}\cdot\text{K}$) [28,29].

4. Conclusion

The presented study reports on the structural and thermal properties of NCD layers grown at low temperatures (below 450°C) by MW-LA-PECVD at different substrate-to-antenna distance (SAD). SEM and topographical AFM maps show a homogeneous NCD layer in samples from #7.5 to #10 SAD, with a roughness (R_a) between 20 and 40 nm and a linear trend of thickness reduction from 420 to 219 nm, respectively. From a distance of #11 onwards, only dispersed NCD clusters are observed with a very low growth rate. This result indicates a limit for high-density plasma to be around 11 cm. Raman spectroscopy shows $>90\%$ sp^3 diamond content in the samples. The growth conditions used do not lead to a high incorporation of boron into the diamond. NCD

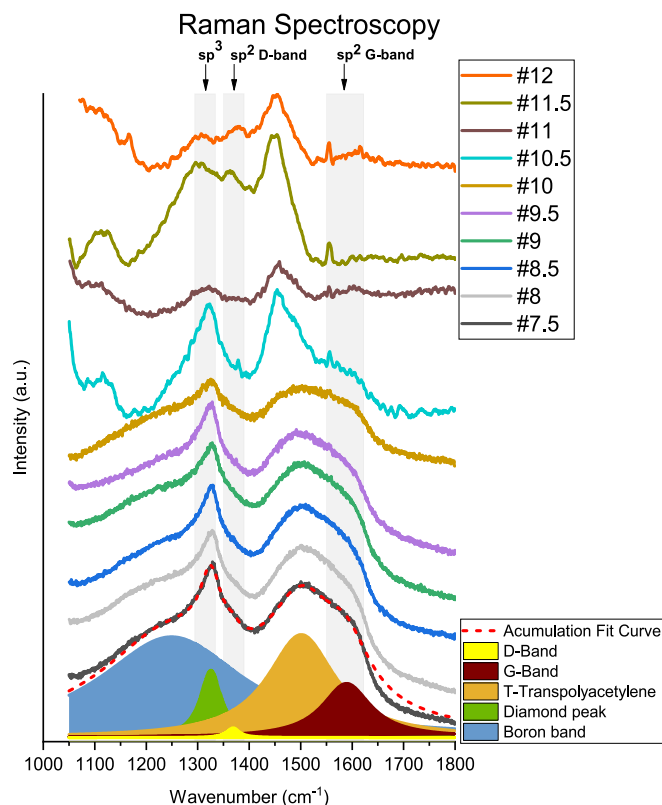


Fig. 3. Raman spectroscopy of nanocrystalline diamond samples grown at different SAD. Samples were grown by MW-LA-PECVD. Spectrum #7.5 was deconvoluted in all bands and peaks, which contribute to the Raman signal. Grey boxes indicate the intervals in which the bands and peaks are located. [44].

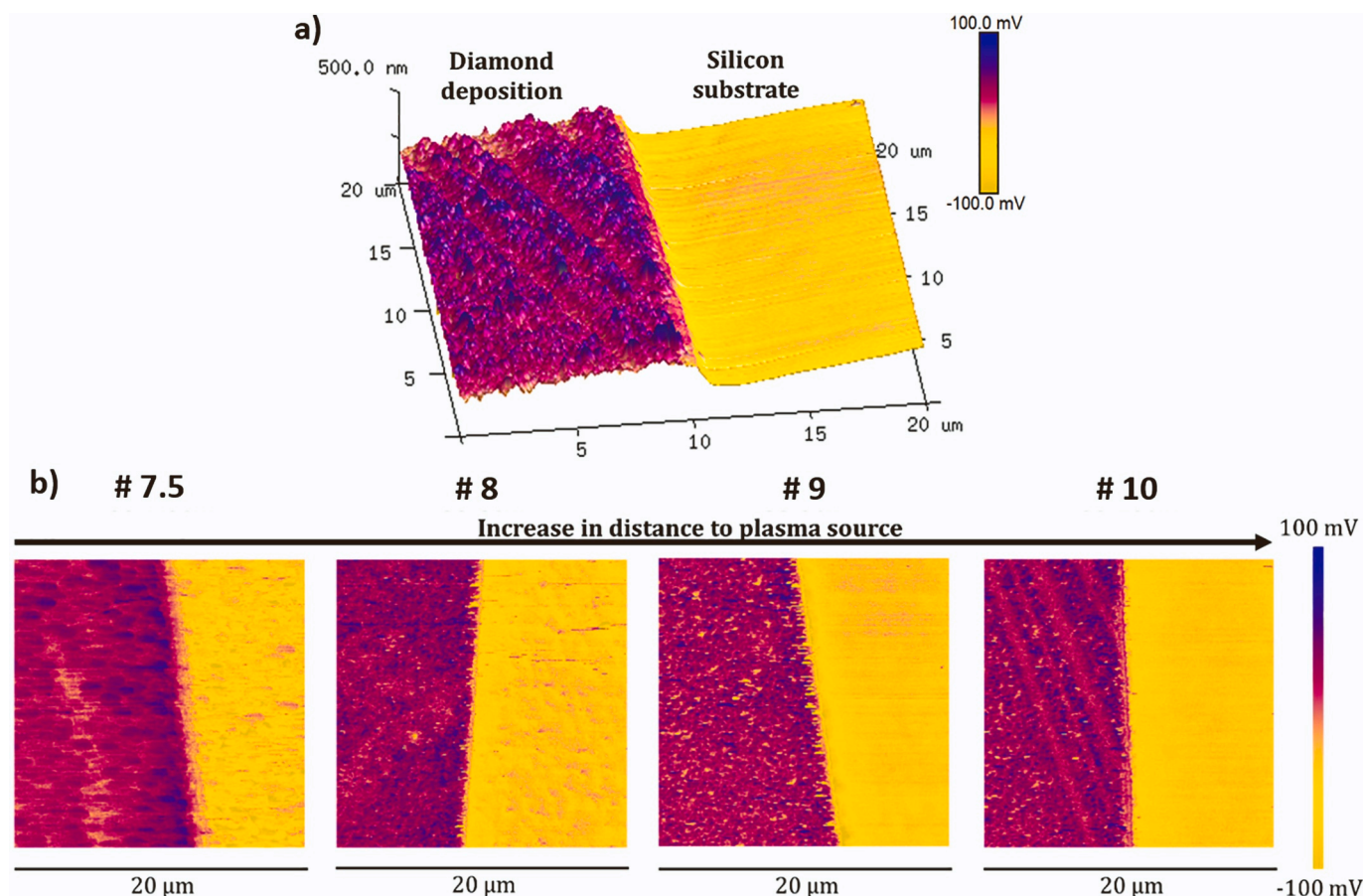


Fig. 4. SThM-AFM results: a) Topography and thermal conductivity map obtained from NCD on Si. b) Thermal conductivity of NCD and Si substrate at different SAD. The purple and yellow regions correspond to NCD and Si, respectively.

Table 1

Analysis of the thermal conductivity distributions of SThM-AFM maps from Fig. 4.

Sample	Distribution peak centre (mV)		NCD Thermal conductivity (W/m•K)	SAD (cm)
	M_{NCD}	M_{Si}		
#7.5	118.9	58.0	97.6 ± 0.5	7.5
#8	123.2	61.6	100.0 ± 0.1	8
#9	136.5	79.5	116.5 ± 0.2	9
#10	129.0	68.2	107.7 ± 0.3	10

thermal conductivity is unaffected by SAD and thickness layer. Superficial thermal conductivity maps on NCD layers using SThM-AFM establishes a thermal conductivity of $\lambda = 10^2$ W/m•K. The thermal conductivity is uniform over the entire NCD surface and independent of the SAD. The nanocrystalline diamond grown at low temperature by MW-LA-PECVD in pulse mode shows thermal conductivity of the same order of magnitude as NCD grown by MWPECVD or HFCVD at higher temperatures (800–1200 °C). The present study frames the thermal characteristics of NCD in large area and low temperature deposition by MW-LA-PECVD to integrate diamond into commercial applications.

Declaration of competing interest

The authors declare the following financial interests/personal relationships which may be considered as potential competing interests: Josue Millan-Barba reports financial support was provided by Foundation for the Research, Development and Application of Composite

Materials.

Data availability

Data will be made available on request.

Acknowledgement

The authors thank to the Ministerio de Economía y Empresa (MINECO) of the Spanish Government for funding under grant N° PID2019-110219RB-I00 and N° PID2020-117201RB-C21, as well as the co-financing by the 2014-2020 ERDF Operational Programme, the funding grants N° PY20_00946 and N° FEDER-UCA18-107851 and by the Department of Economy, Knowledge, Business and University of the Regional Government of Andalusia. M. Dominguez acknowledges the support by the Spanish Ministerio de Ciencia, Innovación y Universidades under project EQC2018-004704-P. They are especially grateful to the Fundación para la Investigación, Desarrollo y Aplicación de Materiales Compuestos - FIDAMC and also to the University of Salamanca.

References

- [1] B. Soto, J. Cañas, M.P. Villar, D. Araujo, J. Pernot, Transport mechanism in O-terminated diamond/ZrO₂ based MOSCAPs, *Diam. Relat. Mater.* 121 (2022) <https://doi.org/10.1016/j.diamond.2021.108745>.
- [2] M. Panizza, G. Cerisola, Application of diamond electrodes to electrochemical processes, *Electrochim. Acta* 51 (2005) 191–199, <https://doi.org/10.1016/j.electacta.2005.04.023>.
- [3] S. Yu, S. Liu, X. Jiang, N. Yang, Recent advances on electrochemistry of diamond related materials, *Carbon* N. Y. 200 (2022) 517–542, <https://doi.org/10.1016/j.carbon.2022.09.044>.

- [4] S. Chauhan, N.G. Jain, U. Nagaich, Nanodiamonds with powerful ability for drug delivery and biomedical applications: recent updates on in vivo study and patents, *J. Pharm. Anal.* 10 (2020) 1–12, <https://doi.org/10.1016/j.jpha.2019.09.003>.
- [5] K. Bobzin, High-performance coatings for cutting tools, *CIRP J. Manuf. Sci. Technol.* 18 (2017) 1–9, <https://doi.org/10.1016/j.cirpj.2016.11.004>.
- [6] K. Yang, W. Chen, Y. Zhao, L. Ding, B. Du, S. Zhang, et al., Enhancing dielectric strength of thermally conductive epoxy composites by preventing interfacial charge accumulation using micron-sized diamond, *Compos. Sci. Technol.* 221 (2022), 109178, <https://doi.org/10.1016/j.compscitech.2021.109178>.
- [7] J.H.T. Luong, K.B. Male, J.D. Glennon, Boron-doped diamond electrode: synthesis, characterization, functionalization and analytical applications, *Analyst.* 134 (2009) 1965–1979, <https://doi.org/10.1039/b910206j>.
- [8] I. Kratochvilova, Polycrystalline diamond thin films for advanced applications, in: *Adv. Carbon Nanostructures*, 2016, pp. 161–173, <https://doi.org/10.5772/64701>.
- [9] A. Taylor, L. Fekete, J. Vl, R. Vladimira, V. Petrak, J. Krucký, et al., Novel high frequency pulsed MW-linear antenna plasma-chemistry: routes towards large area, low pressure nanodiamond growth, *Diam. Relat. Mater.* 20 (2011) 613–615, <https://doi.org/10.1016/j.diamond.2011.01.003>.
- [10] H.A. Mehedi, J. Achard, D. Rats, O. Brinza, A. Tallaire, V. Mille, et al., Low temperature and large area deposition of nanocrystalline diamond films with distributed antenna array microwave-plasma reactor, *Diam. Relat. Mater.* 47 (2014) 58–65, <https://doi.org/10.1016/j.diamond.2014.05.004>.
- [11] M. Ficek, P. Niedzialkowski, M. Śmietana, M. Koba, S. Drijkoningen, R. Bogdanowicz, et al., Linear antenna microwave chemical vapour deposition of diamond films on long-period fiber gratings for bio-sensing applications, *Opt. Mater. Express.* 7 (2017) 3952, <https://doi.org/10.1364/ome.7.003952>.
- [12] M. Ihara, H. Maeno, K. Miyamoto, H. Komiyama, Low-temperature deposition of diamond in a temperature range from 70 °C to 700 °C, *Diam. Relat. Mater.* 1 (1992) 187–190.
- [13] F. Piazza, G. Morell, Synthesis of diamond at sub 300 °C substrate temperature, *Diam. Relat. Mater.* 16 (2007) 1950–1957, <https://doi.org/10.1016/j.diamond.2007.08.038>.
- [14] F. Fendrych, A. Taylor, L. Peksa, I. Kratochvilova, J. Vlcek, V. Rezacova, et al., Growth and characterization of nanodiamond layers prepared using the plasma-enhanced linear antennas microwave CVD system, *J. Phys. D. Appl. Phys.* 43 (2010) 0–6. doi:<https://doi.org/10.1088/0022-3727/43/37/374018>.
- [15] A. Kromka, O. Babchenko, T. Izak, K. Hruska, B. Rezek, Linear antenna microwave plasma CVD deposition of diamond films over large areas, *Vacuum* 86 (2012) 776–779, <https://doi.org/10.1016/j.vacuum.2011.07.008>.
- [16] M. Liehr, S. Wiedner, M. Dieguez-Campo, Large area microwave coating technology, *Thin Solid Films* 502 (2006) 9–14, <https://doi.org/10.1016/j.tsf.2005.07.226>.
- [17] S. Drijkoningen, P. Pobedinskas, S. Korneychuk, A. Momot, Y. Balasubramaniam, M.K. Van Bael, et al., On the origin of diamond plates deposited at low temperature, *Cryst. Growth Des.* 17 (2017) 4306–4314, <https://doi.org/10.1021/acs.cgd.7b00623>.
- [18] J. Zalieckas, I.R. Mondragon, P. Pobedinskas, A.S. Kristoffersen, S. Mohamed-ahmed, C. Gjerde, et al., Polycrystalline diamond coating on orthopedic implants: realization and role of surface topology and chemistry in adsorption of proteins and cell proliferation, *Appl. Mater. Interfaces* 14 (2022) 44933–44946, <https://doi.org/10.1021/acsami.2c10121>.
- [19] J. Kim, K. Tsugawa, M. Ishihara, Y. Koga, M. Hasegawa, Large-area surface wave plasmas using microwave multi-slot antennas for nanocrystalline diamond film deposition, *Plasma Sources Sci. Technol.* 19 (2010) 5, <https://doi.org/10.1088/0963-0252/19/1/015003>.
- [20] B. Baudrillart, F. Bénédict, A.S. Melouani, F.J. Oliveira, R.F. Silva, J. Achard, Low-temperature deposition of nanocrystalline diamond films on silicon nitride substrates using distributed antenna array PECVD system, *Phys. Status Solidi Appl. Mater. Sci.* 213 (2016) 2575–2581, <https://doi.org/10.1002/pssa.201600221>.
- [21] J. Zalieckas, P. Pobedinskas, M. Möller Greve, K. Eikehaug, K. Haenen, B. Holst, Large area microwave plasma CVD of diamond using composite right/left-handed materials, *Diam. Relat. Mater.* 116 (2021), <https://doi.org/10.1016/j.diamond.2021.108394>.
- [22] K. Tsugawa, M. Ishihara, J. Kim, M. Hasegawa, Y. Koga, Large-area and low-temperature nanodiamond coating by microwave plasma, *Chem. Vap. Depos.* 16 (2007).
- [23] K. Tsugawa, M. Ishihara, J. Kim, Y. Koga, M. Hasegawa, Nanocrystalline diamond film growth on plastic substrates at temperatures below 100 °C from low-temperature plasma, *Phys. Rev. B - Condens. Matter Mater. Phys.* 82 (2010) 1–8, <https://doi.org/10.1103/PhysRevB.82.125460>.
- [24] A. Taylor, P. Ashcheulov, P. Hubík, L. Klimša, J. Kopeček, Z. Remeš, et al., Precursor gas composition optimisation for large area boron doped nanocrystalline diamond growth by MW-LA-PECVD, *Carbon N. Y.* 128 (2018) 164–171, <https://doi.org/10.1016/j.carbon.2017.11.063>.
- [25] A. Taylor, L. Fekete, P. Hubík, A. Jäger, P. Janíček, V. Mortet, et al., Large area deposition of boron doped nano-crystalline diamond films at low temperatures using microwave plasma enhanced chemical vapour deposition with linear antenna delivery, *Diam. Relat. Mater.* 47 (2014) 27–34, <https://doi.org/10.1016/j.diamond.2014.05.002>.
- [26] R. Haubner, M. Lessiak, Deposition of CVD diamond coatings on carbon fiber composite substrates, *Key Eng. Mater.* 742 (2017) 419–426, <https://doi.org/10.4028/www.scientific.net/KEM.742.419>.
- [27] E.C. Almeida, M.R. Baldan, J.M. Rosolen, N.G. Ferreira, Impedance characteristics of the diamond/carbon fiber electrodes for electrical double-layer capacitor, *Diam. Relat. Mater.* 17 (2008) 1529–1533, <https://doi.org/10.1016/j.diamond.2008.03.006>.
- [28] J. Anaya, S. Rossi, M. Alomari, E. Kohn, L. Tóth, B. Pécz, et al., Control of the in-plane thermal conductivity of ultra-thin nanocrystalline diamond films through the grain and grain boundary properties, *Acta Mater.* 103 (2016) 141–152, <https://doi.org/10.1016/j.actamat.2015.09.045>.
- [29] L. Saturday, L. Wilson, S. Retterer, N.J. Evans, D. Briggs, P.D. Rack, et al., Thermal conductivity of nano- and micro-crystalline diamond films studied by photothermal excitation of cantilever structures, *Diam. Relat. Mater.* 113 (2021), 108279, <https://doi.org/10.1016/j.diamond.2021.108279>.
- [30] K. Suzuki, Y. Shiraiishi, N. Nakajima, M. Iwai, S. Ninomiya, Y. Tanaka, et al., Development of new PCD made up of boron doped Diamond particles and its machinability by EDM, *Av. Mater. Res.* 76–78 (2009) 684–689, <https://doi.org/10.4028/www.scientific.net/AMR.76-78.684>.
- [31] J.E. Graebner, H. Altmann, N.M. Balzaretti, R. Campbell, H.B. Chae, A. Degiovanni, et al., Report on a second round robin measurement of the thermal conductivity of CVD diamond, *Diam. Relat. Mater.* 7 (1998) 1589–1604, [https://doi.org/10.1016/s0925-9635\(98\)00241-6](https://doi.org/10.1016/s0925-9635(98)00241-6).
- [32] M. Engenhorst, J. Fecher, C. Notthoff, G. Schierning, R. Schmechel, S.M. Risiwal, Thermoelectric transport properties of boron-doped nanocrystalline diamond foils, *Carbon N. Y.* 81 (2015) 650–662, <https://doi.org/10.1016/j.carbon.2014.10.002>.
- [33] O.J.L. Fox, J.O.P. Holloway, G.M. Fuge, P.W. May, M.N.R. Ashfold, Electrospray deposition of diamond nanoparticle nucleation layers for subsequent CVD diamond growth, *Mater. Res. Soc. Symp. Proc.* 1203 (2010) 53–59, <https://doi.org/10.1557/proc-1203-j17-27>.
- [34] M. Marton, M. Vojs, P. Michniak, M. Behúl, V. Rehacek, M. Pifko, et al., New chemical pathway for large-area deposition of doped diamond films by linear antenna microwave plasma chemical vapor deposition, *Diam. Relat. Mater.* 126 (2022), <https://doi.org/10.1016/j.diamond.2022.109111>.
- [35] A. Taylor, L. Fekete, P. Hubík, A. Jager, P. Janíček, V. Mortet, et al., Large area deposition of boron doped nano-crystalline diamond films at low temperatures using microwave plasma enhanced chemical vapour deposition with linear antenna delivery, *Diam. Relat. Mater.* 47 (2014) 27–34, <https://doi.org/10.1016/j.diamond.2014.05.002>.
- [36] T. Izak, O. Babchenko, M. Varga, S. Potocky, A. Kromka, I. Diamond, Low Temperature Diamond Growth by Linear Antenna Plasma CVD Over Large Area 2603, 2012, pp. 2600–2603, <https://doi.org/10.1002/psb.201200103>.
- [37] Š. Potocký, M. Čada, O. Babchenko, T. Izák, M. Davydova, A. Kromka, Perspectives of linear antenna microwave system for growth of various carbon nano-forms and its plasma study, *Phys. Status Solidi Basic Res.* 250 (2013) 2723–2726, <https://doi.org/10.1002/psb.201300085>.
- [38] K. Tsugawa, S. Kawai, M. Ishihara, J. Kim, Y. Koga, H. Sakakita, et al., Nanocrystalline diamond growth in a surface-wave plasma, *Diam. Relat. Mater.* 20 (2011) 833–838, <https://doi.org/10.1016/j.diamond.2011.03.031>.
- [39] P. Ashcheulov, A. Taylor, Z. Vlčková Živcová, P. Hubík, J. Honolka, M. Vondráček, et al., Low temperature synthesis of transparent conductive boron doped diamond films for optoelectronic applications : role of hydrogen on the electrical properties, *Appl. Mater. Today* 19 (2020), <https://doi.org/10.1016/j.apmt.2020.100633>.
- [40] H.A. Bland, E.L.H. Thomas, G.M. Klemencic, S. Mandal, A. Papageorgiou, T. G. Jones, et al., Superconducting diamond on silicon nitride for device applications, *Sci. Rep.* 9 (2019), <https://doi.org/10.1038/s41598-019-39707-z>.
- [41] A.C. Ferrari, J. Robertson, Origin of the 1150 – cm⁻¹ Raman mode in nanocrystalline diamond, *Phys. Rev. B - Condens. Matter Mater. Phys.* 63 (2001) 2–5, <https://doi.org/10.1103/PhysRevB.63.121405>.
- [42] A.C. Ferrari, J. Robertson, Interpretation of Raman spectra of disordered and amorphous carbon, *Phys. Rev. B* 61 (2000) 95–107.
- [43] G.M. Sardonato, K. Iha, Characterization of boron doped CVD diamond films by Raman spectroscopy and X-ray diffractometry, *Diam. Relat. Mater.* 11 (2002) 1578–1583.
- [44] V. Mortet, I. Gregora, A. Taylor, N. Lambert, P. Ashcheulov, Z. Gedeonova, et al., New perspectives for heavily boron-doped diamond Raman spectrum analysis, *Carbon N. Y.* 168 (2020) 319–327, <https://doi.org/10.1016/j.carbon.2020.06.075>.
- [45] J. Vlcek, F. Fendrych, A. Taylor, M. Novotny, M. Liehr, Pulsed plasmas study of linear antennas microwave CVD system for nanocrystalline diamond film growth, *J. Mater. Res.* 27 (2012) 863–867, <https://doi.org/10.1557/jmr.2011.381>.
- [46] J. Vlcek, F. Fendrych, A. Taylor, M. Novotny, M. Liehr, Pulsed plasmas study of linear antennas microwave CVD system for nanocrystalline diamond film growth, *J. Mater. Res.* 27 (2012) 863–867, <https://doi.org/10.1557/jmr.2011.381>.